

Dextrous Manipulation of a Micropart with Multiple Compliant Probes through Visual Force Feedback

John D. Wason, John T. Wen

Center for Automation Technologies & Systems
Rensselaer Polytechnic Institute
Troy, NY 12180
{wasonj,wenj}@rpi.edu

Nicholas G. Dagalakis

Intelligent Systems Division
National Institute of Standards and Technology
Gaithersburg, Maryland 20899-8230
nicholas.dagalakis@nist.gov

Abstract—In our recent work, we have demonstrated effectiveness of the concept of multi-probe microassembly for manipulating and inserting microscale, sub-millimeter, parts to create three-dimensional microstructures. However, the approach has been based on trial-and-error manual teaching of grasp points to ensure a stable grasp during motion. As a result, the part orientation is restricted (nearly aligned with the world reference frame and lying flat) to ensure successful grasping and manipulation. In this paper, we developed a kinematics based hybrid motion and force control based only on vision feedback. We first conduct a systematic analysis of the bending of the probes while they are in contact with the part, to estimate the grasp force based on the vision feedback of the probe configuration. A Jacobian based controller is then used for position manipulation while maintaining the desired squeeze force. Experimental results with two probes and two camera are included to demonstrate the effectiveness of the controller to move the part to specified position and orientation while maintaining sufficient squeeze force to prevent part slippage.

I. INTRODUCTION

Microassembly is a technology that attempts to overcome the inherent limits of monolithic bulk micro-machined micro electro-mechanical system (MEMS) devices. With the increasing precision of sensing and actuation technologies and the need for the assembly of more complex devices, there has been surging interest and research efforts in this area [1]. Many strategies have been proposed; this paper focuses on multi-probe microassembly that manipulates microparts without the use of microgrippers. The specifics of this approach and its advantages have been discussed in our previous work on this topic [2]–[4]. Though the approach has been successfully demonstrated, a critical step in the procedure, stable grasping of the part while performing part manipulation, is based on manual teaching of the grasp points. A great deal of trial and error is required – with too little force, the part cannot be picked up or is dropped; with too

much force, the part flies off like a sling shot. This approach clearly lacks robustness and generality.

This paper presents an automated motion and force control method based on the vision feedback. Vision based microassembly has been used in the past [5], [6], but not for force estimation in 3D microassembly. We analyze the bending of the probe while in contact with the part. This analysis is then used to estimate the contact force based on the vision feedback of the bending of the probe. The estimated force is used in a kinematics-based force control. Vision feedback is also used in the motion control of the part. The two controllers are combined for the manipulation of the part while maintaining the required contact force.

Most of the position and orientation control presented in previous work involves the following scenarios: the part is placed on the surface and pushed by probes [5], [7]–[9], the part is rigidly held by a gripper that fully constrains the part within the gripper [10]–[12], or the orientation of the part is manipulated by probes, but without rigorous control and feedback [7], [13].

The method presented here uses two compliant probes to grasp the part, pressing on either side of the part. The only requirement for the part shape is that it have two parallel surfaces available for gripping. The compliance of the probes is used to form a stable and robust grasp. The probes are moved independently using three mutually orthogonal prismatic joints. (The manipulators are capable of more degrees of freedom but only three are necessary.) The Jacobian for this mechanism is used for the kinematic controller used to implement the motion and force control. Vision feedback is used to measure the position and orientation of the physical part. For the current experiments a $300\ \mu\text{m} \times 300\ \mu\text{m} \times 25\ \mu\text{m}$ part is used, as shown in Figure 1.

II. KINEMATICS BASED MOTION AND FORCE CONTROL

Consider two probes contacting a part as shown in Figure 2. Let C be an Euclidean frame fixed with respect to the part. In this paper, we only use the Cartesian motion of the probes, and the contacts are modeled as point contacts with friction.

This work is supported in part by the National Institute of Standards and Technology (NIST) under the Small Grant program and the Center for Automation Technologies and Systems (CATS) under a block grant from the New York State Office of Science, Technology, and Academic Research (NYSTAR).

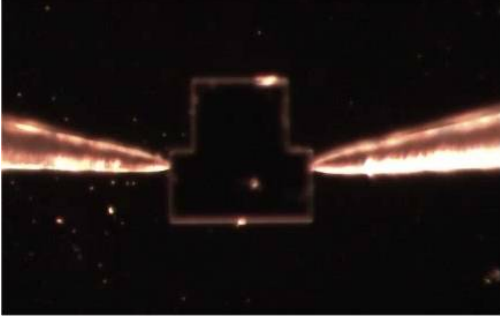


Fig. 1. Micropart used in experiments

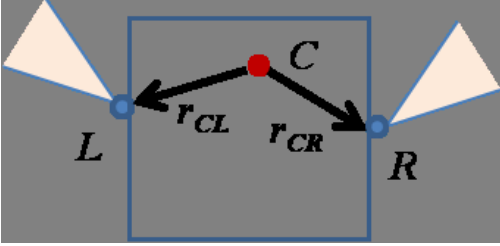


Fig. 2. Kinematics of two probes interacting with a part

The differential kinematics is then given by

$$AV_c = Ju + Hw \quad (1)$$

where

$$A := \begin{bmatrix} A_L \\ A_R \end{bmatrix}, J := \begin{bmatrix} J_L & 0 \\ 0 & J_R \end{bmatrix}, H = \begin{bmatrix} H_L & 0 \\ 0 & H_R \end{bmatrix}$$

$$V_c := \begin{bmatrix} \omega_c \\ v_c \end{bmatrix}, u = \begin{bmatrix} u_L \\ u_R \end{bmatrix}, w = \begin{bmatrix} w_L \\ w_R \end{bmatrix}$$

(ω_c, v_c) is the spatial velocity of C , (u_L, u_R) are the commanded Cartesian velocity of the probes, (w_L, w_R) are the relative rotations between the probes and the part, and

$$A_L = \begin{bmatrix} I_{3 \times 3} & 0_{3 \times 3} \\ -r_{CL} \times & I_{3 \times 3} \end{bmatrix}, A_R = \begin{bmatrix} I_{3 \times 3} & 0_{3 \times 3} \\ -r_{CR} \times & I_{3 \times 3} \end{bmatrix}$$

$$J_L = J_R = \begin{bmatrix} 0_{3 \times 3} \\ I_{3 \times 3} \end{bmatrix}, H_L = H_R = \begin{bmatrix} I_{3 \times 3} \\ 0_{3 \times 3} \end{bmatrix}.$$

Note that A is of full column rank so its left-inverse and annihilator may be written as:

$$A^+ = \frac{1}{2} [A_L^{-1} \quad A_R^{-1}], \tilde{A} = [A_L^{-1} \quad -A_R^{-1}]. \quad (2)$$

To obtain the constraint equation of the closed kinematic chain, we apply \tilde{A} to both sides of (1):

$$\tilde{A}Ju + \tilde{A}Hw = 0. \quad (3)$$

The orientation portion of (3) does not involve u and implies

$$w_L = w_R. \quad (4)$$

The translational portion of (3) is

$$u_L - u_R + r_{CL} \times w_L - r_{CR} \times w_R =$$

$$u_L - u_R + (r_{CL} - r_{CR}) \times w_L = 0 \quad (5)$$

Parameterize w_L (and w_R) as

$$w_L = w_R = [e_{RL} \quad e_{RL_1}^\perp \quad e_{RL_2}^\perp] \begin{bmatrix} w_1 \\ w_2 \\ w_3 \end{bmatrix} \quad (6)$$

where e_{RL} is the unit vector pointing from contact R to contact L , $e_{RL_1}^\perp$ is any unit vector perpendicular to e_{RL} (chosen to be on the plane of the part), and $e_{RL_2}^\perp := e_{RL} \times e_{RL_1}^\perp$. Substituting into (5), we get

$$u_L - u_R = \ell [0 \quad -e_{RL_2}^\perp \quad e_{RL_1}^\perp] \begin{bmatrix} w_1 \\ w_2 \\ w_3 \end{bmatrix} \quad (7)$$

where ℓ is the length of the line segment from L to R . We can now solve for w_2 and w_3 :

$$\begin{bmatrix} w_2 \\ w_3 \end{bmatrix} = \begin{bmatrix} -(e_{RL_2}^\perp)^T \\ (e_{RL_1}^\perp)^T \end{bmatrix} \frac{u_L - u_R}{\ell}. \quad (8)$$

The variable w_1 is arbitrary, corresponding to the null space motion of $\tilde{A}H$ (rotation about the line between the contacts). This degree of freedom allows rotation of the part by pressing the part against the stationary probe [2].

For the part motion, multiply both sides of (1) by A^\dagger to get

$$V_C = A^\dagger Ju + A^\dagger Hw. \quad (9)$$

The rotational portion only depends on w . Using the solution from the constraint equation we have

$$\omega_c = w_L + w_R. \quad (10)$$

Represent ω_c as

$$\omega_c = [e_{RL} \quad e_{RL_1}^\perp \quad e_{RL_2}^\perp] \begin{bmatrix} \omega_{c1} \\ \omega_{c2} \\ \omega_{c3} \end{bmatrix}$$

we have

$$\omega_{c1} = w_1 \quad (11)$$

$$\begin{bmatrix} \omega_{c2} \\ \omega_{c3} \end{bmatrix} = \begin{bmatrix} -(e_{RL_2}^\perp)^T \\ (e_{RL_1}^\perp)^T \end{bmatrix} \frac{u_L - u_R}{\ell} \quad (12)$$

where w_1 corresponds to the rotation about the line between the contacts. The translational portion is given by

$$v_c = \frac{1}{2}(u_L + u_R) + (r_{CL} + r_{CR}) \times \omega_c. \quad (13)$$

If we choose C to be on the line between the contacts, then $r_{CL} + r_{CR}$ is along e_{RL} and, as expected, w_1 will have no effect on v_C . Putting both angular and linear velocities

together (except for ω_{c1} which is not controlled by the probe motion directly), we have (with C chosen along e_{RL}):

$$\begin{bmatrix} \omega_{c2} \\ \omega_{c3} \\ v_c \end{bmatrix} = \underbrace{\begin{bmatrix} -(e_{RL2}^\perp)^T & (e_{RL2}^\perp)^T \\ (e_{RL1}^\perp)^T & -(e_{RL1}^\perp)^T \\ \frac{1}{2}I_{3 \times 3} & \frac{1}{2}I_{3 \times 3} \end{bmatrix}}_{J_T} \begin{bmatrix} u_L \\ u_R \end{bmatrix}. \quad (14)$$

The Jacobian matrix J_T is a 5×6 full column rank matrix. A proportional feedback may be used to control the corresponding orientation and position:

$$\begin{bmatrix} u_L \\ u_R \end{bmatrix} = -J_T^\dagger K_m \begin{bmatrix} \phi - \phi_{des} \\ x_c - x_{c_{des}} \end{bmatrix} \quad (15)$$

where $(x_c, x_{c_{des}})$ are the measured and desired position of C , and (ϕ, ϕ_{des}) are the measured and desired angles corresponding to $(\omega_{c2}, \omega_{c3})$, respectively.

For the squeeze force, first recognize that the contact spatial force (torque and force), $F = [F_L^T \ F_R^T]^T$, is complementary to the contact motion, i.e.,

$$H_L F_L = H_R F_R = 0 \quad (16)$$

or the contact spatial forces only consist of forces:

$$F_L = \tilde{H}_L^T \eta_L, \quad F_R = \tilde{H}_R^T \eta_R \quad (17)$$

where $\tilde{H}_{L/R}$ is the annihilator of $H_{L/R}$:

$$\tilde{H}_L = \tilde{H}_R = \begin{bmatrix} 0_{3 \times 3} & I_{3 \times 3} \end{bmatrix} \quad (18)$$

and η_L and η_R are the contact forces. The forces propagate to C to cause part motion (translation only):

$$\begin{aligned} F_C &= A^T F = A^T \underbrace{\tilde{H}^T}_{\eta} \begin{bmatrix} \eta_L \\ \eta_R \end{bmatrix} \\ &= \begin{bmatrix} r_{CL} \times & r_{CR} \times \\ I_{3 \times 3} & I_{3 \times 3} \end{bmatrix} \begin{bmatrix} \eta_L \\ \eta_R \end{bmatrix}. \end{aligned} \quad (19)$$

The component of the contact force η that does not cause motion (i.e., in the null space of $A^T \tilde{H}^T$) imparts a ‘‘squeeze’’ to the part:

$$\mathcal{N}(A^T \tilde{H}^T) = \gamma \begin{bmatrix} e_{RL} \\ -e_{RL} \end{bmatrix}. \quad (20)$$

A common and effective force control strategy is the integral force feedback, see e.g., [14], where the applied squeeze force control (the control that does not cause motion) is a negative feedback of the measured squeeze force error. Assuming linear compliance of the part, the integral force control becomes

$$u_L = -u_R = -k_f (f_s - f_{s_{des}}) e_{RL} \quad (21)$$

where f_s is the scalar component of the squeeze force η , and $f_{s_{des}}$ is the desired squeeze force level.

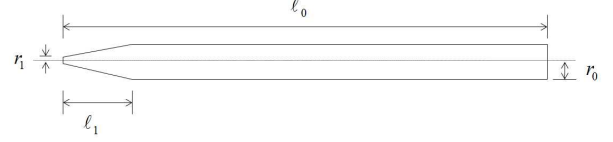


Fig. 3. Diagram of probe shape

Combining the motion and force controllers, (15) and (21), together, we obtain the controller for the probe velocity that we use for grasping, manipulation, and rotation of the part:

$$\begin{bmatrix} u_L \\ u_R \end{bmatrix} = -J_T^\dagger K_m \begin{bmatrix} \phi - \phi_{des} \\ x_c - x_{c_{des}} \end{bmatrix} - k_f \begin{bmatrix} -(f_s - f_{s_{des}}) e_{RL} \\ (f_s - f_{s_{des}}) e_{RL} \end{bmatrix}. \quad (22)$$

The x - y components of the measured part position x_c are obtained from the top camera image. The z component of x_c is obtained from the side camera. The unit vector between the contacts, e_{RL} , is obtained based on the probe tip positions. The desired part orientation and position $(\phi_{des}, x_{c_{des}})$ is specified by the planner for each task primitive. The squeeze force, f_s , is estimated based on probe deformation obtained from vision, as presented in the next section.

III. VISION BASED CONTACT FORCE ESTIMATION

Tungsten probes are used to grasp and manipulate the micro parts being assembled. Tungsten probes are tough, cheap, and have one of the highest Young’s modulus of any available material. The geometry of the probe is as shown in Figure 3. The cross section of the probe is circular. The probe is long compared with its cross section dimension. We can therefore model it as an Euler-Bernoulli beam [15]. In a static equilibrium, the probe deflection is given by

$$\frac{d^2}{dx^2} EI(x) w''(x) = 0, \quad 0 \leq x \leq \ell_0 \quad (23)$$

where w is the bending deflection displacement of the probe at location x , E is the Young’s modulus of Tungsten, $I(x)$ is the area moment of inertia, and ℓ_0 is the length of the probe. The boundary conditions, fixed at $x = \ell_0$ and a transverse force F applied to the probe tip and zero moment at the probe tip $x = 0$, are given as follows:

$$w(\ell_0) = w'(\ell_0) = 0, \quad w''(0) = 0, \quad \frac{dEIw''}{dx}(0) = F \quad (24)$$

where F is the force applied to the probe tip.

From (23), we have

$$EI(x) w''(x) = a_0 + a_1 x$$

for some constants a_0 and a_1 . Applying the boundary conditions at 0, we have

$$EI(x) w''(x) = Fx. \quad (25)$$

Integrating twice and applying the boundary conditions at $x = \ell_0$, we have

$$\begin{aligned} w(x) &= \left[-\int_{\ell_0}^x \left(-\int_{\ell_0}^{\ell} \frac{s}{I(s)} ds \right) dl \right] \frac{F}{E} \\ &= \left[\int_x^{\ell_0} \int_{\ell}^{\ell_0} \frac{s}{I(s)} ds dl \right] \frac{F}{E}. \end{aligned} \quad (26)$$

We are interested in determining the force exerted onto the probe by measuring its tip deflection, $w(0)$, using vision. The tip deflection is related to the applied force by

$$w(0) = \underbrace{\left(\frac{1}{E} \int_x^{\ell_0} \int_{\ell}^{\ell_0} \frac{s}{I(s)} ds dl \right)}_{K_b} F. \quad (27)$$

This relationship holds true for the probe bending in the transverse (y and z) directions.

The loading in the axial, x , direction has two effects. The axial force F_x adds a term $F_x w''$ to the left hand side of (23) which leads to an additional term $F_x w(0)$ in EIw'' . For small deflection, the effect of this term is negligible. An axial force could also lead to axial deformation given by

$$\delta_x(0) = \int_0^{\ell_0} \frac{F_a}{EA(x)} dx \quad (28)$$

where $A(x)$ is the cross-sectional area. The axial stiffness is given by the ratio $K_a = \frac{F_a}{\delta_x(0)}$. For thin rods, K_a is several orders of magnitude larger than K_b . We will therefore assume the probe is infinitely rigid in the axial direction.

The cameras are used to measure the probe tip bending vector δ_b in the probe transverse direction. From the bending stiffness, K_b from (27), the bending force may be estimated as

$$F_b = K_b \delta_b. \quad (29)$$

To find the squeeze force, we solve the force balance at the contact, including the axial force on the probe:

$$F_b + f_a x_{probe} + f_s e_{RL} = 0. \quad (30)$$

Since F_b and x_{probe} are orthogonal, the least square solution is

$$f_s = -\frac{e_{RL}^T F_b}{(1 + x_{probe}^T e_{RL})^2}. \quad (31)$$

When only the top camera is used, only the planar projection of δ_b is measured, i.e.,

$$\delta_b = \delta_{b_{xy}} + \delta_{b_z} z_o \quad (32)$$

where $\delta_{b_{xy}} = (I - z_o^T z_o) \delta_b$ is the measured planar projection of δ_b and δ_{b_z} is an additional unknown of δ_b in the world z direction, z_o . The force balance equation becomes

$$K_b \delta_{b_{xy}} + K_b \delta_{b_z} z_o + f_a x_{probe} + f_s e_{RL} = 0. \quad (33)$$

and may be used to solve for (δ_{b_z}, f_a, f_s) provided (z_o, x_{probe}, e_{RL}) are independent.

The probe configuration should avoid having the axial axis in opposing directions (i.e., e_{RL} and x_{probe} are collinear) as f_s cannot be uniquely determined from (30). This configuration is also undesirable as it does not utilize the compliance of the probe in the bending direction. The high stiffness in the axial direction makes the grasp much less robust, where small misalignment would cause the failure of the grasp.

For our experiment, we have used GGB Industries ST-20-10 model tungsten probes¹. The probe has a circular cross section with shaft diameter $r_0 = 0.255$ mm and tip radius $r_1 = 10$ μ m. The length of the tip portion of the probe is $\ell_1 = 2.8$ mm, tapering linearly from r_0 to r_1 . After clamping, the length of the probe is $\ell_0 = 25.4$ mm. The radius of the probe may be written as:

$$r(x) = \begin{cases} r_1 + \frac{r_0 - r_1}{\ell_1} x & 0 \leq x \leq \ell_1 \\ r_0 & \ell_1 < x \leq \ell_0 \end{cases}. \quad (34)$$

The area moment of inertia for a circular rod is

$$I(x) = \frac{1}{4} \pi r(x)^4. \quad (35)$$

The Young's Modulus of Tungsten is $E = 400$ GPa. The bending stiffness is calculated to be $K_b = 217.6$ N/m and the axial stiffness to be $K_a = 848$ kN/m.

IV. EXPERIMENTAL RESULTS

A. Overview of Microassembly Testbed

The microassembly system used in this research is a combination of hardware and software configured for telerobotic, operator assisted, and fully automated assembly tasks. Several different components have been integrated to produce an effective system. Figure 4 shows the close-up view of the microassembly testbed. The major components of the systems are:

- The probes are mounted on two 3-DOF ThorLab NanoMax 600 positioners in an opposed configuration. (1.2 μ m step size, 2.4 μ m repeatability)
- A 3-DOF die stage (x - y - θ) consisting of Newport CR4524 X-Y stages with EncoderDriver DC motor actuators and an OWIS Qmbh B-0308143X rotational stage with stepper motor. (2 μ m linear accuracy, $< (1 \times 10^{-3})^\circ$ rotation accuracy)
- Two 1.2 Megapixel C-mount microscope Firewire cameras with actuated zoom. These cameras are both Basler A631F cameras. The top camera has an actuated collimated 16 \times precision zoom lens. The side camera uses an Edmund VZM450 zoom lens. The Basler A631F Firewire camera has a maximum resolution of (1392 \times 1040) pixels, with a large 1/2" progressive scan CCD array. When combined with the zoom lens, it

¹Certain commercial products and processes are identified in this paper to foster understanding. Such identification does not imply recommendation or endorsement by the National Institute of Standards and Technology, nor does it imply that the products and processes identified are necessarily the best available for the purpose.

provides a working resolution of between $3\ \mu\text{m}$ and $1.5\ \mu\text{m}$ depending on the zoom level. The lenses have been augmented with stepper motors to provide automated zoom capabilities. These lenses have a constant working distance over the entire zoom range. One camera is configured as an overhead camera, while another camera provides a side view approximately 20 degrees off horizontal.

- Control electronics and MATLAB and Visual Basic based software interface

The system is designed around two actuated probe manipulators operating over a silicon die containing the device being assembled. The two manipulators are sharp-tipped probes ($20\ \mu\text{m}$ diameter) designed to manipulate small silicon parts. The probes are mounted on two 3-DOF stepper translational stages with about $1.2\ \mu\text{m}$ positional accuracy. The die itself is mounted on a 3-DOF (planar translation and rotation) stage mounted between the two probe stages. The die stage allows the die to be moved into and out of the relatively limited work space of the probes – the range of motion in any direction is only approximately 4 mm. With the combination of the motion of the probes and the motion of the die, manipulation can take place at any location on the $10\ \text{mm}\times 10\ \text{mm}$ die. The kinematic relationship between the various components in the system is determined through an automated vision based calibration procedure [2].

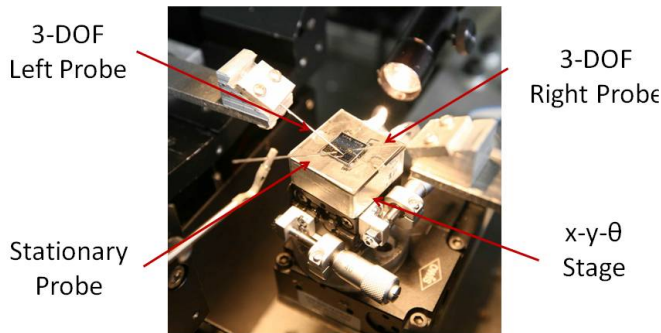


Fig. 4. Close-up View of the Microassembly Experimental Testbed

B. Motion and Force Control Experiments

In the example experiment, we conduct two moves that requires coordinated motion and force control. The first move involves using the the probes grasping the part, lifting it up by about $80\ \mu\text{m}$ and centering it (with the mid-point of the part at $x = y = 0\ \mu\text{m}$ and $\theta = 0^\circ$, the rotation angle about z). The second move involves moving the mid-point of the part to $x=80\ \mu\text{m}$, $y=-80\ \mu\text{m}$, and rotating the part by $\theta=15^\circ$. Throughout the move, the force set point is set at 5 mN. This force setpoint was selected based on experience from previous experiments. The motion and force results for the moves are shown in Figure 5–6. The position converges to the specified set point in each motion segment.

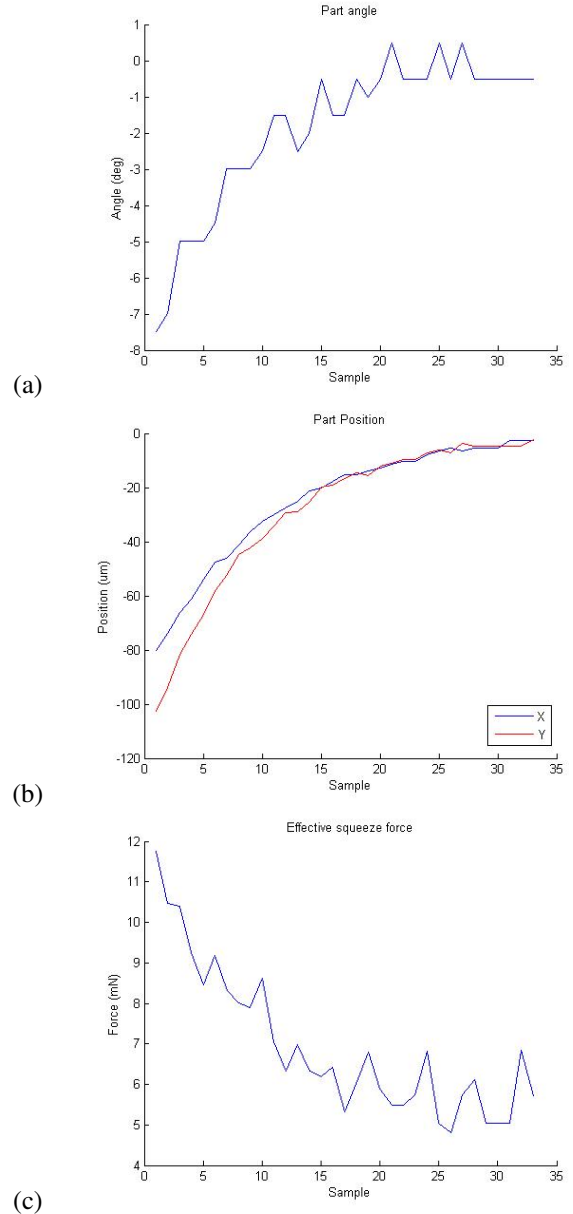


Fig. 5. First motion (a) angle (b) position (c) grip force vs sample

The force converges to the force set point in the first segment and maintains around the set point in the second segment. The force is estimated by measuring the deflection of the probe using the cameras. This procedure is noisy and only provides a coarse measurement, so the estimated value shows some level of oscillation. However, the force measurement is sufficient for a stable grasp, as shown in the experiment. Due to the camera resolution and probe motion resolution limits, the final positioning accuracy is less than $5\ \mu\text{m}$ for the prismatic directions and less than 0.1° for the part orientation. The video attached to this paper shows the grasp, and the two motion segments.

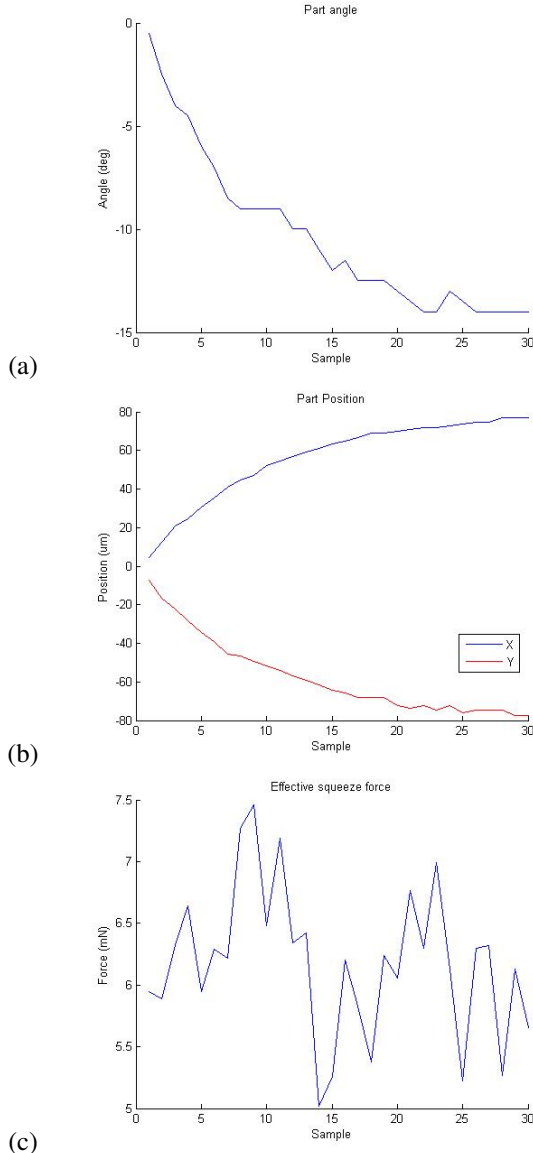


Fig. 6. Second motion (a) angle (b) position (c) grip force vs sample

V. CONCLUSION

This paper has presented the quasi-static grasp mechanics and a two dimensional controller for kinematics-based position and grasp force control. By using only vision feedback, we have demonstrated that it is possible to execute dexterous manipulation of the part while maintaining adequate control of the contact force. While the controller and experiment presented are two dimensional, the concepts presented may be extended to the spatial case. Currently the limiting factor is the ability to fully resolve the orientation of a part in three

dimensions. A new camera configuration is under consideration that will allow for the part to be oriented precisely and installed in the desired position on the substrate in full 3D.

ACKNOWLEDGMENT

This work was supported in part by the Center for Automation Technologies and Systems (CATS) under a block grant from the New York State Foundation for Science, Technology and Innovation (NYSTAR), in part by the National Institute of Standards and Technology (NIST), and in part by the National Science Foundation (NSF) Smart Lighting Engineering Research Center (EEC-0812056).

REFERENCES

- [1] M. Gauthier and S. Régnier, *Robotic micro-assembly*. Wiley-IEEE Press, 2010.
- [2] J. D. Wason, W. T. Gressick, J. T.-Y. Wen, J. J. Gorman, and N. G. Dagalakis, "Multi-probe micro-assembly," in *Third Annual IEEE Conference on Automation Science and Engineering*, Scottsdale, AZ, 2007.
- [3] J. D. Wason, W. T. Gressick, J. T.-Y. Wen, J. J. Gorman, and N. G. Dagalakis, "Multiprobe microassembly experimental testbed," in *International Conference on Micromanufacturing*, Pittsburg, PA, 2008.
- [4] J. D. Wason, J. T. Wen, Y.-M. Choi, J. J. Gorman, and N. G. Dagalakis, "Vision guided multi-probe microassembly of 3d microstructures," in *IEEE/RSJ International Conference on Intelligent Robots and Systems*, Taipei, Taiwan, October 2010.
- [5] A. Ferreira, C. Cassier, and S. Hirai, "Automatic microassembly system assisted by vision servoing and virtual reality," *IEEE/ASME Transactions on Mechatronics*, vol. 9, no. 2, pp. 321–333, June 2004.
- [6] B. Tamadazte, N. L.-F. Piat, and S. Dembl, "Robotic micromanipulation and microassembly using monoview and multiscale visual servoing," *IEEE/ASME Transactions on Mechatronics*, vol. 16, no. 2, pp. 277 – 287, 2011.
- [7] E. Shimada, J. Thompson, J. Yan, R. Wood, and R. Fearing, "Prototyping millirobots using dextrous microassembly and folding," in *ASME Symposium on Microrobotics*, 2000.
- [8] J. Thompson and R. Fearing, "Automating microassembly with orthotweezers and force sensing," in *IEEE/RSJ International Conference on Intelligent Robots and Systems*, vol. 3, 2001.
- [9] D. Cappelleri, J. Fink, B. Mukundakrishnan, V. Kumar, and J. Trinkle, "Designing open-loop plans for planar micro-manipulation," in *IEEE Int. Conf. on Robotics and Automation, Orlando, FL*, 2006.
- [10] B. N. G. Yang, J.A. Gaines, "Optomechatronic design of microassembly systems for manufacturing hybrid microsystems," in *IEEE Transactions on Industrial Electronics*, 2005, pp. 1013–1023.
- [11] N. Dechev, L. Ren, W. Liu, W. Leghorn, and J. Millis, "Development of a 6 degree of freedom robotic micromanipulator for use in 3d mems microassembly," in *IEEE International Conference on Robotics and Automation*, 2006, pp. 281–288.
- [12] D. Popa, W. Lee, R. Murthy, A. Das, and H. Stephanou, "High yield automated mems assembly," in *IEEE International Conference on Automation Science and Engineering*, 2007, pp. 1099–1104.
- [13] T. Tanikawa and T. Arai, "Development of a micro-manipulation system having a two-fingered micro-hand," *IEEE Transactions on Robotics and Automation*, no. 1, Feb. 1999.
- [14] L. Wilfinger, J. Wen, and S. Murphy, "Integral force control with robustness enhancement," *IEEE Control System Magazine*, vol. 14, no. 1, pp. 31–40, Feb. 1994.
- [15] L. Meirovitch, *Analytic Methods in Vibration*. New York: The MacMillan Company, 1967.